

1 **SUBSURFACE EXPRESSION OF A TERTIARY SALT WELD, GULF OF MEXICO**

2
3 **Christopher A-L. Jackson^{1*}**

4 **Yue Zhang¹**

5 **Donald A. Herron²**

6 **Peter J.R. Fitch¹**

7
8 ¹*Basins Research Group (BRG), Department of Earth Science and Engineering,*
9 *Imperial College London, UK*

10
11 ²*Consultant, Sugar Land, Texas, USA*

12
13
14 *Corresponding author email: c.jackson@imperial.ac.uk

15
16 **ABSTRACT**

17
18 Salt welds form due to expulsion and thinning of salt. Despite welds being ubiquitous in salt-bearing
19 sedimentary basins, where they may trap large volumes of hydrocarbons, we know relatively little of
20 their thickness and composition. We here use 3D isotropic Kirchhoff prestack depth migrated (KPSDM)
21 seismic, borehole, and biostratigraphic data from the Atwater Valley protraction area of the Gulf of
22 Mexico to constrain the thickness and composition of a tertiary salt weld. Seismic data image an
23 ‘apparent weld’ (*sensu* Wagner and Jackson, 2011) at the base of a Plio-Pleistocene minibasin that
24 subsided into thick allochthonous salt. Well data indicate the weld is in fact ‘incomplete’, being c. 24
25 m thick, and containing an upper 5 m thick halite and a lower 15 m thick halite, separated by a 4 m
26 thick mudstone. The age and origin of the intra-weld mudstone is unclear, although we speculate it is:
27 (i) Late Jurassic, representing material transported upwards from the autochthonous level within a
28 feeder, and subsequently trapped as allochthonous salt thinned and welded, or; (ii) Pliocene,
29 representing a piece of carapace material transported upwards atop and reworked from the crest of a
30 feeder that fed the overlying, now-welded sheet. We show that even relatively modern, high-quality 3D
31 seismic reflection data may be unable to resolve salt weld thickness, with the presence of a relatively
32 thin remnant salt lending support to models of welding based on viscous flow. Furthermore, the halite-
33 dominated character of the weld supports the hypothesis that tectonic purification occurs during flow
34 of salt from autochthonous to allochthonous levels.

35
36 **INTRODUCTION**

38 Salt welds are ubiquitous in salt-bearing sedimentary basins, forming due to the complete expulsion of
39 salt from below or between minibasins (Jackson and Cramez, 1989). Salt welds are economically
40 important because, depending on their thickness and composition, they may represent barriers to fluid
41 flow, and thus seal and help trap hydrocarbon accumulations (Rowan, 2004). Furthermore, weld
42 thickness and composition reveal much about salt rheology and patterns of internal deformation
43 (Kupfer, 1968; Wagner and Jackson, 2011; Jackson et al., 2014). Despite their importance and ubiquity,
44 we have a rather poor understanding of the thickness or composition of subsurface welds; in some
45 basins, this reflects a lack of borehole penetrations or, in relatively densely drilled basins, such as the
46 Gulf of Mexico, a lack of access to these data. Where these data are available, such as in the Santos
47 Basin, offshore Brazil they indicate that even high-quality 3D seismic reflection data may be unable to
48 resolve the thickness or composition of welds, and that, at the primary weld level at least, welds may
49 lack true ‘salt’, being halite- and potash-poor, being instead dominated by carbonate, anhydrite, and
50 sandstone (Jackson et al., 2014; see also fig. 17 in Wagner and Jackson, 2011). This lithological
51 partitioning suggests preferential expulsion of halite and potash salt from the autochthonous layer into
52 flanking diapirs during viscous flow and welding. This process, which is termed ‘differential
53 purification by movement’ by Kupfer (1968), implies that successive periods of salt flow, for example
54 as salt ascends from autochthonous to allochthonous levels, will lead to relative enrichment in the more
55 mobile components (e.g. halite, potash salts) of the original salt layer. This observation supports
56 analytical and numerical models based on viscous-thinning of the salt during welding (Wagner and
57 Jackson, 2011), which conclude it is difficult to fully remove salt from a weld by viscous flow alone
58 because of boundary drag along the salt contacts (see also Cohen and Hardy, 1996; Hudec and Jackson,
59 2007). More specifically, the models of Wagner and Jackson (2011) suggest that a weld may contain
60 anywhere from <1 m to up to c. 50 m of remnant salt, although they recognize that model-based
61 predictions of remnant evaporite thickness in salt welds has hitherto been difficult to test due to a lack
62 of data from natural welds (see Wagner, 2010; Hoetz et al., 2011; Liro and Holdaway, 2011; Rowan et
63 al., 2012).

64

65 We here use 3D seismic reflection, borehole and biostratigraphic data from Block 8 in the Atwater
66 Valley protraction area of the Gulf of Mexico (Fig. 1) to characterisation the subsurface expression of
67 a tertiary salt weld. 3D seismic data allow us to define the geophysical expression and regional
68 geological context of the weld, whereas borehole data allow us to constrain weld thickness and
69 composition. Biostratigraphic data provide a rare opportunity to establish the precise age of the weld
70 and subjacent strata, and to place the development of the weld and overburden in the context of the
71 regional salt-tectonic framework. More specifically, our data allow us to explicitly test the following
72 two hypotheses: (i) that allochthonous salt should be relatively enriched in the more mobile lithologies
73 typically encountered at autochthonous levels; and (ii) that only several tens of metres of remnant salt
74 should remain in a seismically defined weld.

75
76
77
78
79
80
81
82
83
84
85
86
87
88
89
90
91
92
93
94
95
96
97
98
99
100
101
102
103
104
105
106
107
108
109
110
111

GEOLOGICAL SETTING

The Gulf of Mexico formed in response to Triassic-Early Cretaceous rifting (e.g., Pindell and Dewey, 1982; Kneller and Johnson, 2011; Hudec et al., 2013b). Extension and subsidence allowed establishment of a restricted marine seaway, within which the Louann salt (Middle Jurassic) was deposited (e.g., Hazzard et al., 1947; Humphris, 1978; Salvador, 1987; Kneller and Johnson, 2011; Hudec et al., 2013a). Since then, in the northern Gulf of Mexico, this salt layer has been flowed to form a complex array of salt diapirs and sheets, canopies and welds, largely in response to loading of the autochthonous and then allochthonous salt levels by Mesozoic to Cenozoic sediments that are now preserved in a series of predominantly clastic-filled minibasins (Fig. 1B) (e.g., Diegel et al., 1995; Peel et al., 1995; Rowan, 1995; Pilcher et al., 2011).

Our study area is located in Block 8 of the Atwater Valley protraction area, on the south-western flank of the Mississippi Fan, northern Gulf of Mexico (Fig. 1). Water depths range from 650 to 1150 m. Here, the salt-tectonic framework is dominated by: (i) Miocene and older rocks contained in primary minibasins that overlie autochthonous salt; (ii) a series of diapiric feeders that separate primary minibasins and that connect upward to and feed salt sheets forming part of a regionally extensive canopy extending southwards to the Sigsbee Escarpment; and (iii) Plio-Pleistocene rocks contained in secondary minibasins that subsided into allochthonous salt and that locally welded to underlying primary minibasins (Fig. 1B).

DATASET

Seismic Data

The seismic volume used in this study is a subset of a large regional 3D survey, composed of multiple narrow-azimuth 3D seismic data sets acquired in 1995-1998 and subsequently reprocessed as a single survey in 2008. This subset covers an area of approximately 550 km² in the southwestern Mississippi Canyon (MC) and northwestern Atwater Valley (AT) protraction areas in the east-central Gulf of Mexico (Fig. 1A). 3D isotropic Kirchhoff prestack depth migrated (KPSDM) data, with a sample rate of 10 m, record length of 15 km, and final bin size of 25m x 25 m, were used for interpretation. The data were processed to zero phase, and all seismic displays in this paper follow a polarity convention in which, for a zero-phase wavelet, a positive reflection coefficient is represented by a central trough (plotted white on a variable-density display).

Borehole Data

112
113
114
115
116
117
118
119
120
121
122
123
124
125
126
127
128
129
130
131
132
133
134
135
136
137
138
139
140
141
142
143
144
145
146
147
148

We use data from exploration borehole AT-8 #1, which was drilled in 1997 in the eastern part of the study area (Fig. 2). The borehole penetrated clastic overburden, before penetrating the studied weld and terminating in underlying clastic rocks. Conventional borehole measurements include differential caliper, bulk density, sonic, gamma ray and neutron porosity, which together allow us to interpret the lithology of the weld, in addition to the sub- and suprasalt strata. Biostratigraphic data are also available in this borehole, allowing us to constrain the age of strata above and below the weld, and thus the weld itself.

METHODOLOGY

Well-to-Seismic Tie and Seismic Interpretation

We identified and mapped three key seismic horizons; (i) base allochthonous salt; (ii) top allochthonous salt; and (iii) top suprasalt mudstone (see below), in addition to the seabed (Figs 3). By mapping base allochthonous salt we were able to identify structural lows at the base of the sheet, which may represent feeders (Fig. 3A) (see Jackson and Hudec, 2017). Mapping top (Fig. 2B) and base (Fig. 2A) salt allowed us to construct a salt isopach (Fig. 2C), from which we identified areas of thin or welded salt. An overburden isopach, generated from our map of top salt and seabed, revealed the location of secondary minibasins and their relationship to the identified salt weld (Fig. 2D).

Well-log Interpretation

We establish the thickness and composition of the salt weld via petrophysical analysis of wireline log data (cf. Jackson et al., 2014). We use a combination of logs to broadly differentiate between: (i) relatively coarse-grained, likely sandstone-prone lithologies; (ii) relatively fine-grained, likely mudstone-dominated lithologies; and (iii) non-clastic lithologies (e.g. evaporites) (Fig. 5) (Rider and Kennedy, 2011). We show that halite is characterised by relatively low GR values (60 - 75 API), low DT values (101 – 125 $\mu\text{s}/\text{ft}$), and low RHOB values (1.99 – 2.11 $\text{g}\cdot\text{cm}^{-3}$). Sandstone occurring above and below the salt is also characterised by low GR values (50 - 70 API), but has moderate DT values (110 – 130 $\mu\text{s}/\text{ft}$) and RHOB values (1.99 – 2.23 $\text{g}\cdot\text{cm}^{-3}$). Mudstone is differentiated from sandstone based on its relatively high GR values (50 – 110 API), moderate to high DT values (116 – 130 $\mu\text{s}/\text{ft}$) and RHOB values (2.14 – 2.31 $\text{g}\cdot\text{cm}^{-3}$). We use the caliper log to identify poor borehole conditions, which may signify intervals of strata deformed due to flow of salt (left-hand log track in Fig. 4A and B) (cf. Hilchie, 1968; Theys, 1999).

Biostratigraphic Analysis

149

150 We calibrate biostratigraphic data from AT-8 to the biostratigraphic chart of the Gulf of Mexico
151 Offshore Region, which is provided by the Bureau of Ocean Energy Management, Regulation and
152 Enforcement from the United States Department of Interior
153 (<https://www.data.boem.gov/Paleo/Files/biochart.pdf>; webpage accessed 15th November 2017). This
154 chart covers regional and local markers, foraminiferal, planktonic and benthic markers, in addition to
155 regional and local calcareous nannoplanktonic markers, spanning the Jurassic to Quaternary.

156

157 **SEISMIC ANALYSIS OF THE SALT-TECTONIC STRUCTURE**

158

159 Here we provide a brief description of the salt-tectonic structure of the study area and the structural
160 context of the weld, focusing on the three main structural units: (i) sub-salt minibasins; (ii)
161 allochthonous salt; and (iii) supra-salt minibasins.

162

163 **Sub-salt Minibasins**

164

165 Due to migration noise and residual multiples generated by overlying allochthonous salt, sub-salt
166 minibasins are not well imaged in our seismic data. Locally, however, where overlying salt is relatively
167 thin, we observe relatively continuous, variable amplitude, sub-horizontal to gently dipping reflections
168 (Fig. 3). These reflections are truncated below allochthonous salt (or its equivalent weld) across a base
169 salt unconformity that is typically steepest near inferred feeders (Fig. 3; see also below). In the
170 northeastern part of the study area, immediately north of AT-8 #1, gently south-dipping strata within a
171 sub-salt minibasin are truncated northward below more steeply dipping strata in a secondary minibasin;
172 we interpret that the contact between these two minibasins is a secondary weld (Fig. 3E) (*sensu* Jackson
173 and Cramez, 1989). AT-8 #1 penetrates the upper 163 m of a sub-salt minibasin, with well-log data
174 (Fig. 4) indicating it contains a broadly continuous, conformable succession of Late Miocene to Late
175 Pliocene deep-water clastics (Fig. 3E).

176

177 **Allochthonous Salt**

178

179 Several allochthonous salt bodies are present within the study area. The tops and bases of these bodies
180 are characterised by regionally mappable, high-amplitude peak (positive) and trough (negative)
181 reflections, respectively. The salt is itself characterised by very chaotic, low-amplitude reflections (Figs
182 3 and 6). The main allochthonous salt body is up to 5500 m thick, broadly U-shaped within the area
183 imaged by our seismic data, and encircles at least the southern end of the minibasin penetrated by AT-
184 8 #1 (Fig. 2C). Base salt is very rugose, being defined by at least five sub-circular structural lows that
185 are up to 8 km in diameter and with up to 2 km of relief (Figs 2A and 3); although subsalt seismic

186 imaging is poor, based on (i) their geometric similarity to features observed elsewhere in the Gulf of
187 Mexico (e.g. Pilcher et al., 2011); (ii) their development at the base of a large allochthonous salt body;
188 and (iii) their development adjacent to clearly truncated sub-salt strata, we interpret these features as
189 the tops of diapiric feeders that rose from autochthonous levels, between and thus defining the sub-salt
190 minibasins, and which fed the overlying allochthonous salt canopy (Jackson and Hudec, 2017).
191 Allochthonous salt appears to locally welded; we describe the geophysical and geological expression
192 of this weld below.

193

194 **Supra-salt Minibasins**

195

196 At least six, at least partially connected supra-salt minibasins overlie the allochthonous salt (i.e.
197 minibasins 1-5) or its equivalent weld (i.e. minibasin 6) (see labels in Fig. 2D). These minibasins are
198 up to 12 km wide and 6.5 km thick, with borehole data indicating they contain Plio-Pleistocene deep-
199 water clastics (Fig. 4).

200

201 **BOREHOLE EXPRESSION OF THE WELD AND SUPERJACENT STRATA**

202

203 A salt weld, which we will later show is ‘apparent’, (terminology after Wagner and Jackson, 2011; see
204 also Jackson et al., 2014), is developed in the east-central part of the study area (Fig. 2E, 3B and E).
205 The weld is defined by two closely spaced seismic reflections, the uppermost being a positive (white)
206 event defining a downward increase in impedance; this seismic response is consistent with acoustically
207 soft, clastic-dominated sedimentary rocks in the supra-salt minibasin overlying acoustically harder,
208 evaporite-dominated rocks within the weld (Fig. 6; see also P-wave log in Fig. 4 and data in Fig. 5).
209 Immediately adjacent to AT-8 #1, the weld dips *c.* 28° southward and is thus conformable with
210 underlying and overlying, broadly south-dipping reflections (Figs 3E and 6B). Directly below the weld,
211 a *c.* 180 m thick package of relatively discontinuous, locally chaotic reflections is present, which is
212 underlain by more continuous reflections (Fig. 6). North of AT-8 #1, the weld dips northward and
213 steepens to *c.* 30°, cross-cutting the discontinuous/chaotic reflections described above, and separating
214 sub- and suprasalt strata, truncating the former at a relatively high-angle (*c.* 45°) (Fig. 6B).

215

216 AT-8 #1 penetrates the central part of minibasin 5 and its underlying weld (Figs 2E, 3B, 3E, and 6).
217 Log data from this borehole thus allow us constrain the petrophysical expression, thickness and
218 composition of the weld (Fig. 4). At the approximate depth of the weld, as defined by our seismic
219 mapping and tied to well control using a regional anisotropy-depth function for correction of seismic
220 depths to well depths, well log data indicate that two anomalously low density, high neutron, low
221 gamma ray intervals are present, separated by a 4 m thick mudstone (4412–4436 m; Fig. 4B). These
222 upper and lower, anomalously low-density intervals, which are 5 m and 15 m thick respectively, plot

223 toward the top-left of a standard neutron–density crossplot (the purple and pink points in Fig. 5), thus
224 are petrophysically and, we infer below, compositionally distinct from the over- and underlying, clastic-
225 dominated sequences. We also observe significant increases in the resistivity log measurements in these
226 intervals (4–16 ohm.m; Fig. 4B), in addition to a relative increase in the ‘change in caliper’
227 measurement, which implies a ‘softer’ lithology that caused enlargement of the borehole during drilling
228 (between 4412–4416 and 4425–4436 m; Fig. 4B). Based on these wireline log-derived observations, in
229 addition to the broader salt-tectonic framework, we interpret that the petrophysically distinct intervals
230 encountered between 4412–4436 m are halite. An alternative interpretation is that these intervals
231 represent gas-bearing clastic rocks; however, we dismiss this interpretation based on the absence of gas
232 indicators at deeper or shallower levels within the borehole. It is important to note that no
233 biostratigraphic data were recovered in this interval, thus the age of the intra-weld mudstone is
234 unknown.

235

236 Our petrophysical analysis indicates that the *c.* 180 m thick package of discontinuous seismic reflections
237 directly below the weld is mudstone-dominated, having similar petrophysical characteristics to shallow
238 and deeper mudstones (i.e. relatively high gamma-ray, high density and moderate porosity; Figs 4 and
239 5).

240

241 **DISCUSSION**

242

243 **The geophysical and geological expression of salt welds**

244

245 We have shown that good quality seismic reflection data can constrain the gross position of a
246 subhorizontal tertiary salt weld. Seismic data cannot, however, determine the completeness or
247 composition of the weld studied here, with borehole data indicating a few tens of metres of halite-
248 dominated stratigraphy remain (cf. Jackson et al., 2014). Recognizing a complete weld or the
249 composition of an incomplete weld may, therefore, be extremely challenging in the absence of borehole
250 data, and incomplete welds might be erroneously interpreted as being complete, when in reality, a thin
251 veneer of impermeable rock remains between adjacent country rocks. The results of our study support
252 the recommendation of Jackson et al. (2014), who suggested that, until borehole data unequivocally
253 demonstrate the absence of evaporite between flanking strata, the term ‘apparent weld’ be used to
254 describe seismically defined welds.

255

256 Our observation that a *c.* 20 m thick sequences remains in the Atwater Valley salt weld is consistent
257 with the predictions of analytical and numerical models presented by Wagner and Jackson (2011),
258 which suggest natural salt welds formed by viscous flow alone may contain anywhere from $\ll 1$ m to
259 up to *c.* 50 m of remnant salt. Our data, and that from the Campos (Wagner and Jackson, 2011) and

260 Santos basins (Jackson et al., 2014), thus support the hypothesis of Wagner and Jackson (2011) that
261 viscous flow is a good analytical approximation of the physical processes occurring during salt thinning
262 and welding, but that viscous flow alone is unlikely to result in complete evacuation of a salt layer.
263 However, it is important to note that a borehole, irrespective of the quantity and quality of data it
264 provides, is only have a 1D sample point; it is possible that, away from this sample point, the weld may
265 be complete.

266

267 **Composition of salt welds**

268

269 Our borehole data indicate the incomplete tertiary weld penetrated by AT-8 #1 is dominated by halite,
270 and that other evaporite (e.g. anhydrite, potash salts) and non-evaporite lithologies, such as carbonate,
271 are absent (Fig. 4). The composition of the weld differs strongly to that encountered in primary welds
272 in the other salt-bearing sediment basins. For example, the Parati Weld, Santos Basin, offshore SE
273 Brazil, which is 22 m thick, is halite-poor, being dominated by carbonate (40%) and anhydrite (40%),
274 with minor amounts of sandstone (16%) and marl (4%). Similarly, halite-poor sequences are observed
275 in incomplete primary welds penetrated by boreholes in the Campos Basin, offshore Brazil (see fig. 17
276 in Wagner and Jackson, 2011). In that location, 75 boreholes have penetrated multi-layered evaporites
277 in the Retiro Member of the Lagoa Feia Formation (Aptian) (or its nonmarine equivalent). Forty-one of
278 these boreholes penetrate evaporite-bearing sequences that are <100 m thick; of these, only 10 boreholes
279 contain halite and anhydrite, with the remaining 31 boreholes containing only anhydrite.

280

281 The compositional variability encountered in primary and tertiary salt welds may reflect several factors,
282 such as compositional variations in the autochthonous salt or preferential dissolution of mobile halite
283 and bittern salts. For example, autochthonous salt comprising solely halite will only yield halite welds.
284 An alternative interpretation is that compositional variability reflects a compositional and, more
285 specifically, rheological control on the rate and ultimately magnitude of expulsion of different
286 lithologies during salt thinning. For example, low viscosity lithologies, such as halite and potash salt,
287 occurring in thick autochthonous salt in relatively large quantities, may be preferentially expelled from
288 thinning salt before relatively high viscosity lithologies, such as carbonate, anhydrite and sandstone. As
289 such, during welding, salt becomes relatively enriched in these less mobile, non-halite lithologies,
290 which, due to the effects of boundary drag along the upper and low salt contacts, becomes trapped in
291 the weld as the salt thinned (compare ‘differential purification by movement’; Kupfer, 1968; see also
292 Wagner and Jackson, 2011 and Jackson et al., 2014). Salt structures flanking welds should thus be
293 relatively enriched in mobile halite and potash salts, an observation that can be made indirectly inferred
294 from seismic facies analysis (Van Gent et al., 2011; Fiduk and Rowan, 2012; Strozyk et al., 2012) or
295 directly proven by borehole data (Jackson et al., 2014; 2015).

296

297 The differential purification by movement model suggests increasing compositional fractionation of
298 salt should occur as the salt tectonic system evolves, with more viscous and/or denser units being
299 stranded within the autochthonous level, trapped in primary welds, or stranded near the basal root of
300 diapirs, and less viscous and/or less dense units forming the cores of these diapirs and, potentially,
301 genetically related, allochthonous sheets and canopies. As such, supra-sheet/canopy minibasins should
302 subside into ‘purer’ salt, comprised largely of halite and potash salts and, accordingly, underlying
303 tertiary welds should be relatively rich in these rock types. Our data support this model, with a halite-
304 rich weld being observed at relatively shallow levels in this salt-tectonic system. However, due to a lack
305 of deep borehole data and post-depositional salt flow, we do not know the composition of autochthonous
306 salt in the Gulf of Mexico, thus we cannot prove the halite-rich nature of the weld described here simply
307 reflects strain-induced compositional fractional.

308

309 Although halite-dominated, the tertiary weld we describe here does contain a 4 m thick mudstone,
310 which, despite being thin, accounts for 17% of the total weld ‘fill’. The origin of this intra-weld
311 mudstone is enigmatic; it may be the same age as the salt (i.e. Jurassic) and have ascended from
312 autochthonous levels (if it is positively buoyant or, at least, not significantly denser than the salt), or be
313 younger (i.e. post-Jurassic) carapace material (thin roof) from the initial feeder, which was then
314 reworked from the crest of the sheet as it advanced, being trapped in spreading and then welding salt.

315

316 **Implications for petroleum systems development in salt basins**

317

318 This observation, along with the fact that various lithologies may remain in an incomplete weld, may
319 directly impact hydrocarbon prospectivity in salt-tectonic basins. For example, the sealing capacity of
320 an incomplete weld containing very low-permeability halite is likely to be higher than an incomplete
321 weld containing permeable layers of carbonates and clastics. We may therefore speculate that primary
322 welds, which may contains relatively little low-permeability halite and thus higher proportions of more
323 permeable non-evaporitic lithologies, may be poorer seals and thus more susceptible to leakage.
324 Additional data from primary, secondary, and tertiary welds, in addition to information on the
325 hydrocarbon presence (or absence) in sub-salt strata, is required to test this hypothesis.

326

327 **CONCLUSIONS**

328

329 3D isotropic Kirchhoff prestack depth migrated (KPSDM) seismic data image the salt-tectonic structure
330 and reveal the geophysical expression of a tertiary salt weld in the Atwater Valley protraction area of
331 the Gulf of Mexico. This weld formed at the base of a Plio-Pleistocene minibasin that subsided into a
332 thick allochthonous salt canopy fed by several diapiric feeders. Seismic reflection data suggest the weld
333 is devoid of salt and is thus ‘complete’, although borehole data demonstrate the weld is in fact

334 'incomplete', being *c.* 24 m thick and containing an upper 5 m thick halite and a lower 15 m thick halite,
335 separated by a 4 m thick mudstone of unknown age. The origin of the intra-weld mudstone is unclear,
336 although it may be Late Jurassic, representing material transported upwards from the autochthonous
337 level within a feeder, or Pliocene, representing carapace material incorporated into the canopy prior to
338 thinning and welding. We show that even relatively modern 3D seismic reflection data may not resolve
339 salt weld thickness, with the presence of a relatively thin layer of evaporites supporting analytically
340 derived models of welding based on viscous flow. Furthermore, the halite-dominated character of the
341 weld supports the hypothesis that tectonic purification occurs during flow of salt from autochthonous
342 to allochthonous levels. In terms of hydrocarbon exploration, understanding the thickness and
343 composition of material left in salt welds is important, with data presented here and in other studies
344 suggesting that, for the same given thickness, the seal potential of tertiary welds may be higher than
345 that of primary (or secondary) welds due to them being relatively enriched in low-permeability halite.

346

347 **ACKNOWLEDGEMENTS**

348

349 We thank Petroleum Geo-Services (PGS) for permission to use and show their proprietary seismic data,
350 and Schlumberger for providing Petrel software to Imperial College via an Academic License
351 Agreement. Biostratigraphic data for the AT-8 #1 were provided by Lexco Data Systems, L. P. in
352 conjunction with Petroleum Geo-Services (PGS). We thank Mike Hudec, Yikuo Liu, and Connor
353 O'Sullivan for very helpful discussions during the course of this study.

354

355 **REFERENCES**

356

357 Cohen, H.A., Hardy, S., 1996. Numerical modelling of stratal architectures resulting from differential
358 loading of a mobile substrate, in G.I. Alsop, D.J. Blundell, and I. Davison, eds., Salt tectonics:
359 Geological Society London Special Publications, 100, 265–273.

360

361 Diegel, F. A., J. F. Karlo, D. C. Schuster, R. C. Shoup, and P.R. Tauvers, 1995, Cenozoic structural
362 evolution and tectono-stratigraphic framework of the northern Gulf Coast continental margin, in M. P.
363 A. Jackson, D. G. Roberts, and S. Snelson, eds., Salt tectonics: A global perspective: AAPG Memoir
364 65, 109–151.

365

366 Fiduk, J.C., and M.G. Rowan, 2012, Analysis of folding and deformation within layered evaporites in
367 Blocks BM-S-8 & -9, Santos Basin, Brazil, in G.I. Alsop, S.G. Archer, A.J. Hartley, N.T. Grant, and R.
368 Hodgkinson, eds., Salt tectonics, sediments and prospectivity: Geological Society of London Special
369 Publications, 363, 471-487.

370

371 Hazzard, R. T., W. C. Spooner, and B. W. Blanpied, 1947, Notes on the stratigraphy of the formations
372 which underlie the Smackover Limestone in south Arkansas, northeast Texas, and north Louisiana:
373 Shreveport Geological Society, Reference Report on Certain Oil and Gas Fields of North Louisiana,
374 South Arkansas, Mississippi and Alabama, vol. II, 483–503.
375

376 Herron, D.A., 2011. First steps in seismic interpretation. Society of Exploration Geophysicists.
377

378 Hilchie, D.W. (1968). Caliper Logging – theory and practice. *The Log Analyst*, 9 (1), p. 3-12.
379

380 Hoetz, G., J. Steenbrinkl, N. Bekkers, A. Vogelaar, and S. Luthi, 2011, Salt-induced stress anomalies:
381 an explanation for variations in seismic velocity and reservoir quality: *Petroleum Geoscience*, 17, 385-
382 396.
383

384 Hudec, M.R., and M.P.A. Jackson, 2007, Terra infirm: understanding salt tectonics: *Earth-Science*
385 *Reviews*, 82, 1-28.
386

387 Hudec, M. R., M. P. A. Jackson, and F. J. Peel, 2013a, Influence of deep Louann structure on the
388 evolution of the northern Gulf of Mexico: *AAPG Bulletin*, 97, 1711–1735.
389

390 Hudec, M. R., I. O. Norton, M. P. A. Jackson, and F. J. Peel, 2013b, Jurassic evolution of the Gulf of
391 Mexico salt basin: *AAPG Bulletin*, 97, 1683–1710.
392

393 Humphris, C. C., Jr., 1978, Salt movement on continental slope, northern Gulf of Mexico, in A. H.
394 Bouma, G. T. Moore, and J. M. Coleman, eds., *Framework, facies, and oil-trapping characteristics of*
395 *the upper continental margin: AAPG*, vol. 7, of, *Studies in Geology*, 69–86.
396

397 Jackson, C.A-L, Rodriguez, C.R., Rotevatn, A., and Bell R.E., 2014, Geological and geophysical
398 expression of a primary salt weld: An example from the Santos Basin, Brazil, *Interpretation*, Vol: 2,
399 Pages: SM77-SM89.
400

401 Jackson, C.A-L., Jackson, M.P.A., Hudec, M.R., and Rodriguez, C.R., 2015, Enigmatic structures
402 within salt walls of the Santos Basin—Part 1: Geometry and kinematics from 3D seismic reflection and
403 well data. *Journal of Structural Geology*, 75, 135-162.
404

405 Jackson, M.P.A., and C. Cramez, 1989, Seismic recognition of salt welds in salt tectonic regimes:
406 *Proceedings of the GCSSEPM Foundation 10th Annual Bob F. Perkins Research Conference*, 66-71.
407

408 Jackson, M.P. and Hudec, M.R., 2017. Salt Tectonics: Principles and Practice. Cambridge University
409 Press.
410

411 Kneller, E. A., and C.A. Johnson, 2011, Plate kinematics of the Gulf of Mexico based on integrated
412 observations from the Central and South Atlantic: Gulf Coast Association of Geological Societies
413 Transactions, 61, 283–300.
414

415 Kupfer, D.H., 1968, Relationship of internal and external structure of salt domes. In: J. Braunstein, and
416 G.D. O'Brien, eds., Diapirism and diapirs: AAPG Memoir, 8, 79–89.
417

418 Liro, L., and S.M. Holdaway, 2011, Salt welds in the deepwater Gulf of Mexico – Uncertainties in the
419 amount of remnant salt: seismic and well examples: AAPG Abstracts with Programs, 986760, p113.
420

421 Peel, F. J., C. J. Travis, and J. R. Hossack, 1995, Genetic structural provinces and salt tectonics of the
422 Cenozoic offshore U.S. Gulf of Mexico: A preliminary analysis: AAPG Memoir, 65, 153–175.
423

424 Pilcher, R.S., Kilsdonk, B. and Trude, J., 2011. Primary basins and their boundaries in the deep-water
425 northern Gulf of Mexico: Origin, trap types, and petroleum system implications. AAPG bulletin, 95(2),
426 pp.219-240.
427

428 Pindell, J., and J.F. Dewey, 1982, Permo-Triassic reconstruction of western Pangea and the evolution
429 of the Gulf of Mexico/Caribbean region: Tectonics, 1, 179–211.
430

431 Rider, M. and Kennedy, M. (2011). The Geological Interpretation of Well Logs (3rd ed.). Rider-French
432 Consulting Ltd, Scotland.
433

434 Rowan, M. G., 1995, Structural styles and evolution of allochthonous salt, central Louisiana outer shelf
435 and upper slope, in M. P. A. Jackson, D. G. Roberts, and S. Snelson, eds., Salt tectonics: A global
436 perspective: AAPG Memoir 65, 199–228.
437

438 Rowan, M.G., 2004, Do salt welds seal? Proceedings of the GCSSEPM Foundation 24th Annual Bob
439 F. Perkins Research Conference (Salt-Sediment Interactions and Hydrocarbon Prospectivity: Concepts,
440 Applications, and Case Studies for the 21st Century), 390-403.
441

442 Rowan, M.G., Lawton, T.F., Giles, K.A., 2012, Anatomy of an exposed vertical salt weld and flanking
443 strata La Popa Basin, Mexico. in G.I. Alsop, S.G. Archer, A.J. Hartley, N.T. Grant, and R. Hodgkinson,
444 eds., Salt tectonics, sediments and prospectivity: Geological Society of London Special Publications,

445 363, 33-57.
 446
 447 Salvador, A., 1987, Late Triassic-Jurassic paleogeography and origin of Gulf of Mexico Basin: AAPG
 448 Bulletin, 71, 419–451.
 449
 450 Strozyk, F., H. Van Gent, J.L. Urai, and P.A. Kukla, 2012, 3D seismic study of complex intra-salt
 451 deformation: An example from the Upper Permian Zechstein 3 stringer, western Dutch offshore, in G.I.
 452 Alsop, S.G. Archer, A.J. Hartley, N.T. Grant, and R. Hodgkinson, eds., Salt tectonics, sediments and
 453 prospectivity: Geological Society of London Special Publications, 363, 489-501.
 454
 455 Theys, P. (1999). Log Data Acquisition and Quality Controls (2nd ed.). Editions Technip, Paris
 456
 457 Van Gent, H., J.L. Urai, and M. de Keijzer, 2011, The internal geometry of salt structures – a first look
 458 using 3D seismic data from the Zechstein of the Netherlands: Journal of Structural Geology, 33, 292-
 459 311.
 460
 461 Wagner III, B.H., 2010, An analysis of salt welding: Unpublished PhD dissertation, University of Texas
 462 at Austin, 218pp.
 463
 464 Wagner III, B.H., and M.P.A. Jackson, 2011, Viscous flow during salt welding: Tectonophysics, 510,
 465 309-326.

467 **FIGURE CAPTIONS**

468
 469 **Fig. 1.** (A) Simplified map showing the location of the study area. The location of the geoseismic profile
 470 shown in Fig. 1B is indicated. (B) Broadly NNW-trending geoseismic profile showing the approximate
 471 structural position and tectono-stratigraphic context of the study area. p=primary weld; t=tertiary weld.
 472 Note that no secondary welds are shown on this profile. TMM=top Middle Miocene; TPL=top Pliocene.
 473 The location of the profile is shown in Fig. 1A. Note that this line lies c. 50 km west of the study area
 474 (see Fig. 1A).

475
 476 **Fig. 2.** (A) base salt depth map; (B) top salt depth map; (C) salt isopach; and (D) post-salt isopach.
 477 Locations of mapped seismic horizons shown in (A) and (B) are shown on Fig. 3.

478
 479 **Fig. 3.** Broadly E-trending seismic profiles through the (A) north, (B) centre, and (C) south of the study
 480 area. (B) intersects through the studied salt weld and borehole AT-8 #1; (D) Broadly N-trending seismic
 481 profiles in the (D) west and (E) east of the study area. (D) and (E) intersects postulated salt feeders (Fig.

482 2E), with (E) also intersecting the studied salt weld and borehole AT-8 #1. s=secondary weld; t=tertiary
483 weld. The locations of Fig. 6A and B are shown in (B) and (E), respectively.

484

485 **Fig. 4.** (A) Well-log and lithology data from the depth interval 4300-4500 m in AT-8 #1. The entire
486 non-evaporitic sedimentary succession shown here is Upper Pliocene. Note the halite-rich character of
487 the weld. For location of borehole, see Figs 2, 3B and D. (B) Details of the well-log expression of
488 interval 4400-4500 in AT-8 #1. The weld and the main lithological subdivisions are indicated, with the
489 colour-code referring to colours indicated in Fig. 5. The seismic polarity convention used for these
490 seismic profiles and those in Fig. 6 are shown in (A).

491

492 **Fig. 5.** Neutron-density cross-plot of petrophysical data from the depth interval 4300-4500 m in AT-8
493 #1. Note the distinct expression of intra-weld halite, which is characterised by significantly lower
494 neutron values than underlying or overlying clastics.

495

496 **Fig. 6.** (A) N-trending seismic profile (IL44638) through borehole AT-8 #1; (B) E-trending profile
497 (XL6602) through borehole AT-8 #1. Both profiles illustrate the seismic character of the salt weld, and
498 overlying and underlying stratigraphy. Note the distinctly chaotic seismic facies directly underlying the
499 weld. The location of (A) is shown in Fig. 3B and the location of (B) in Fig. 3E.

Fig. 1

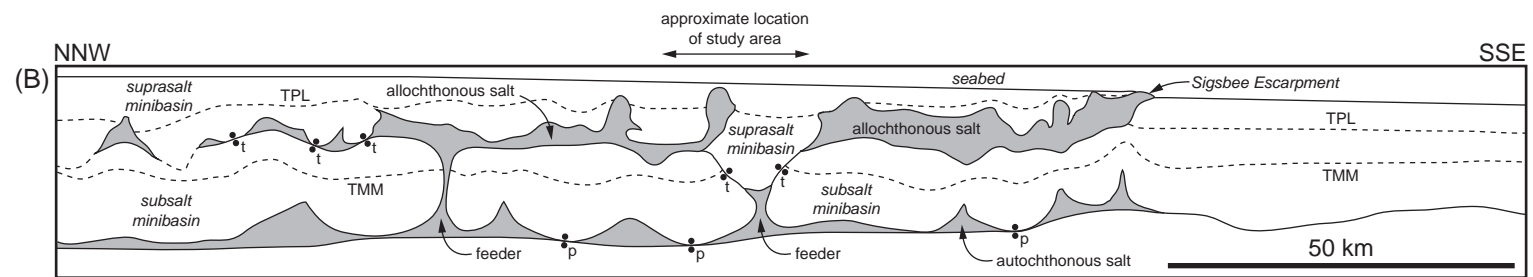
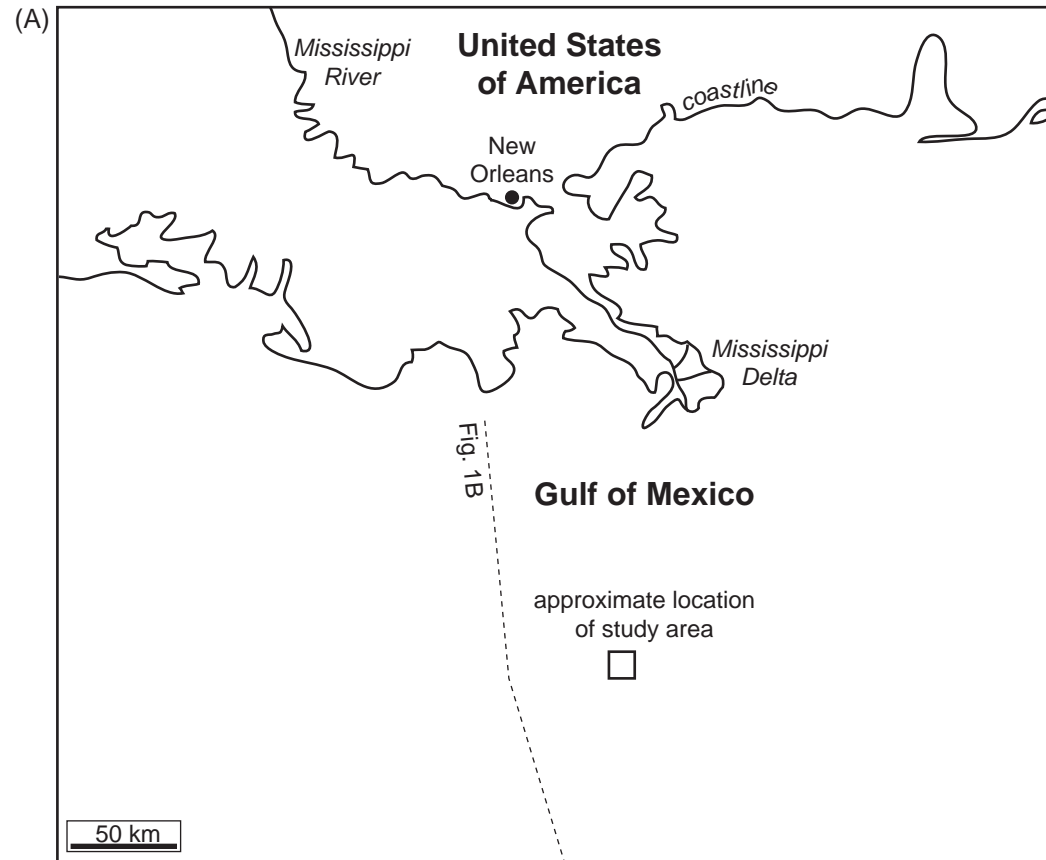


Fig. 2

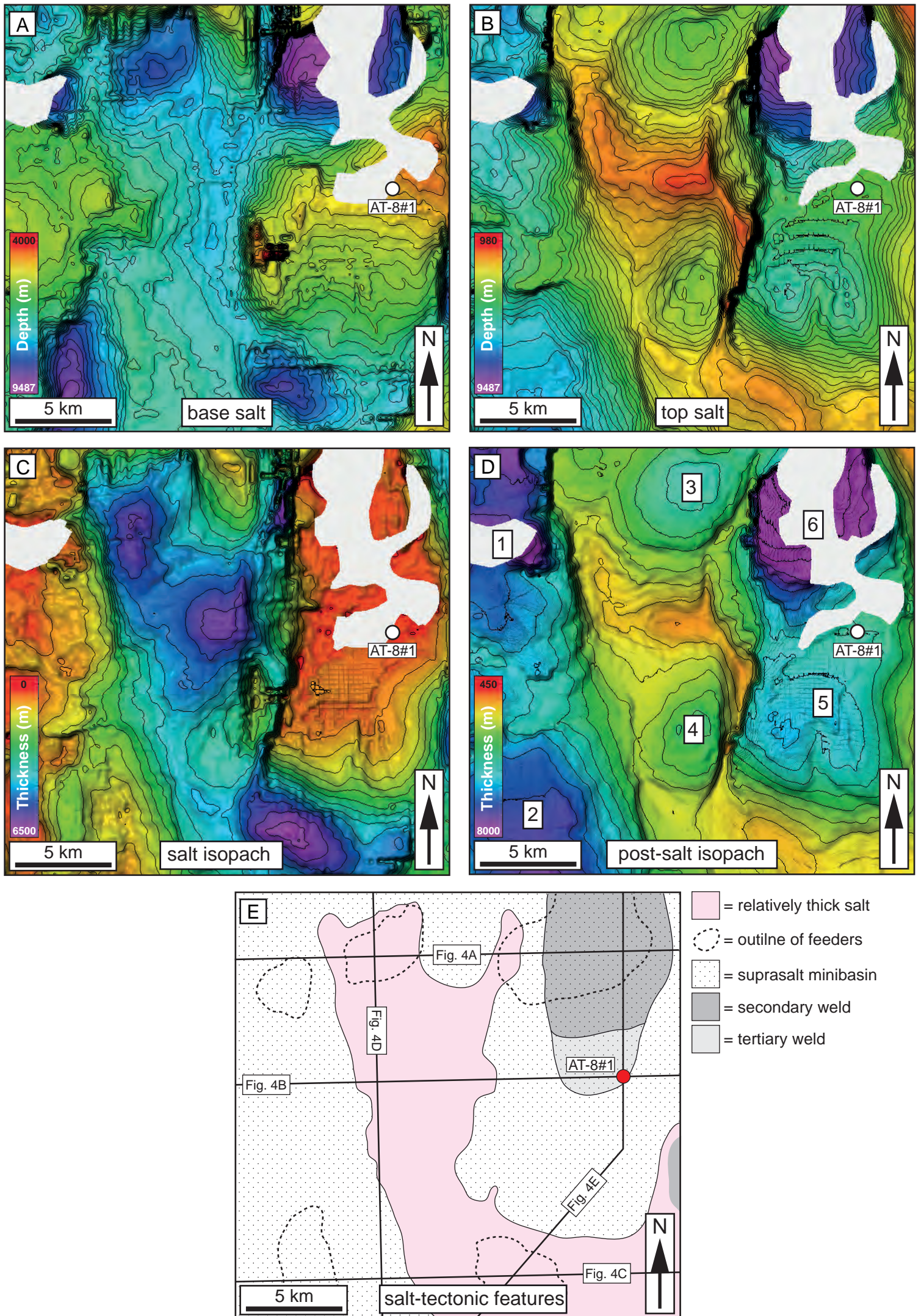


Fig. 3

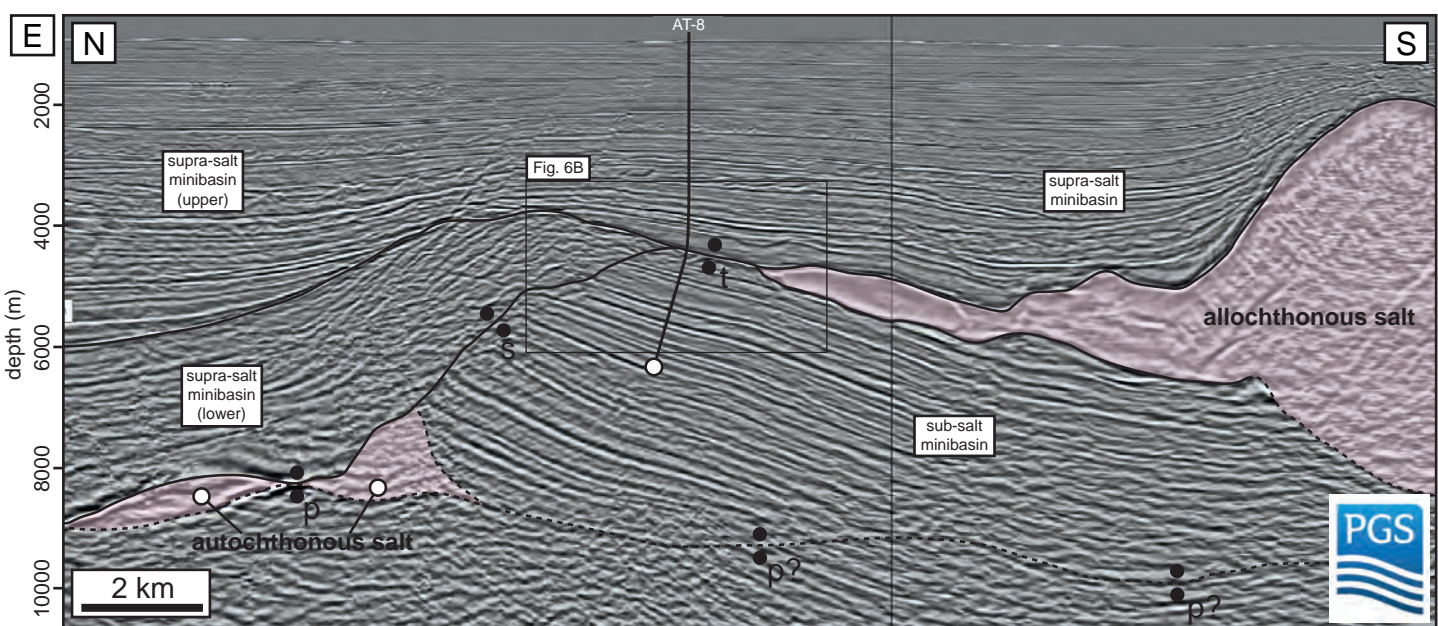
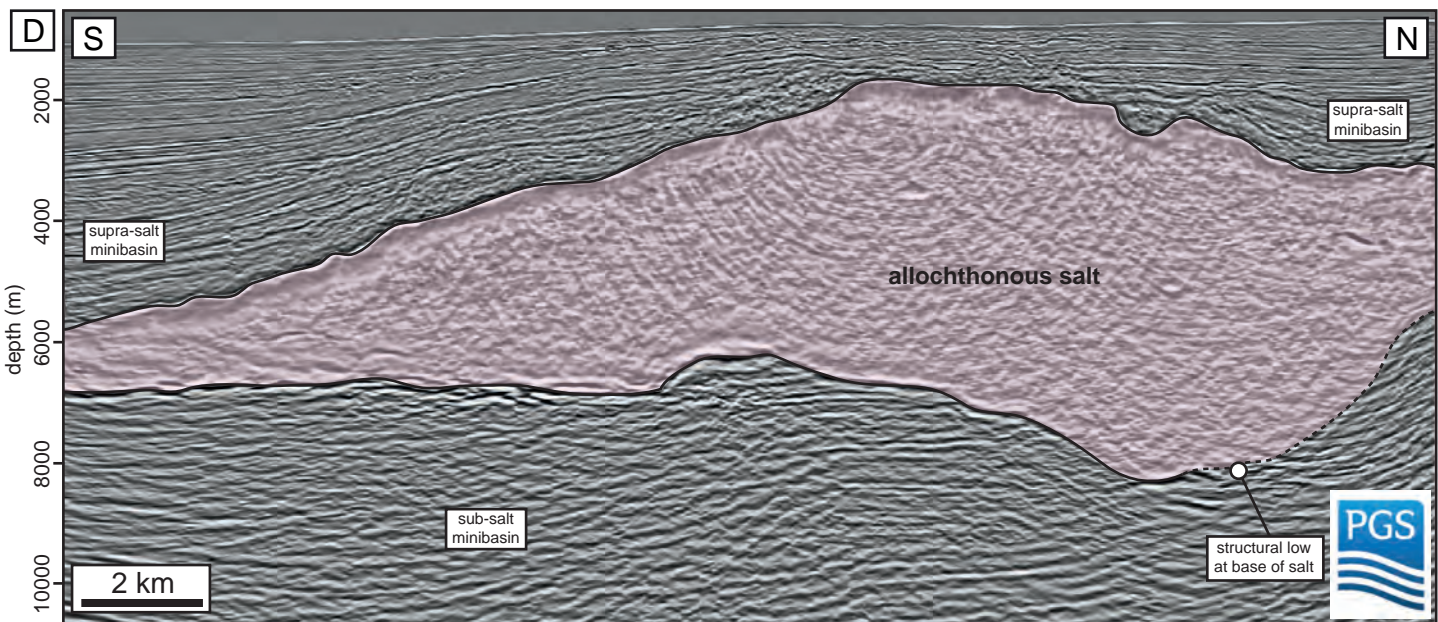
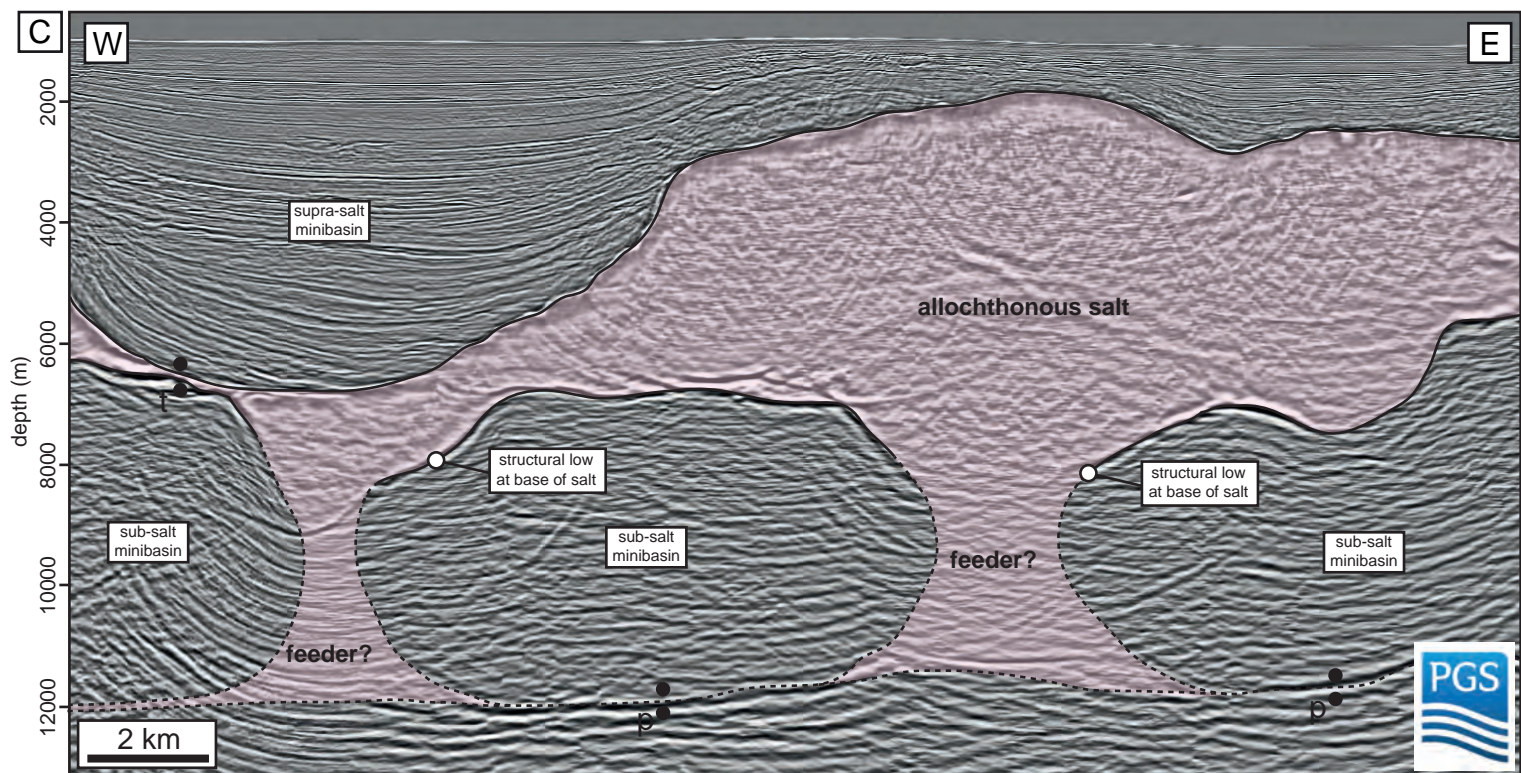
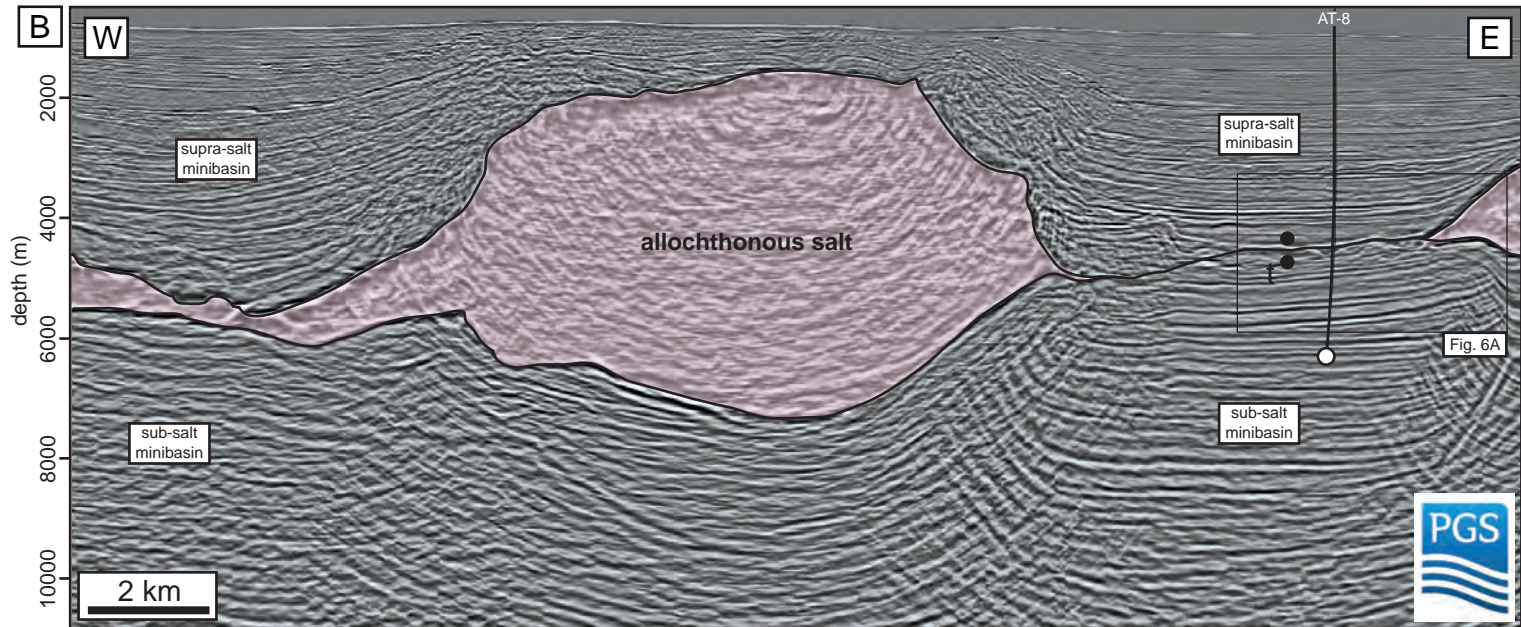
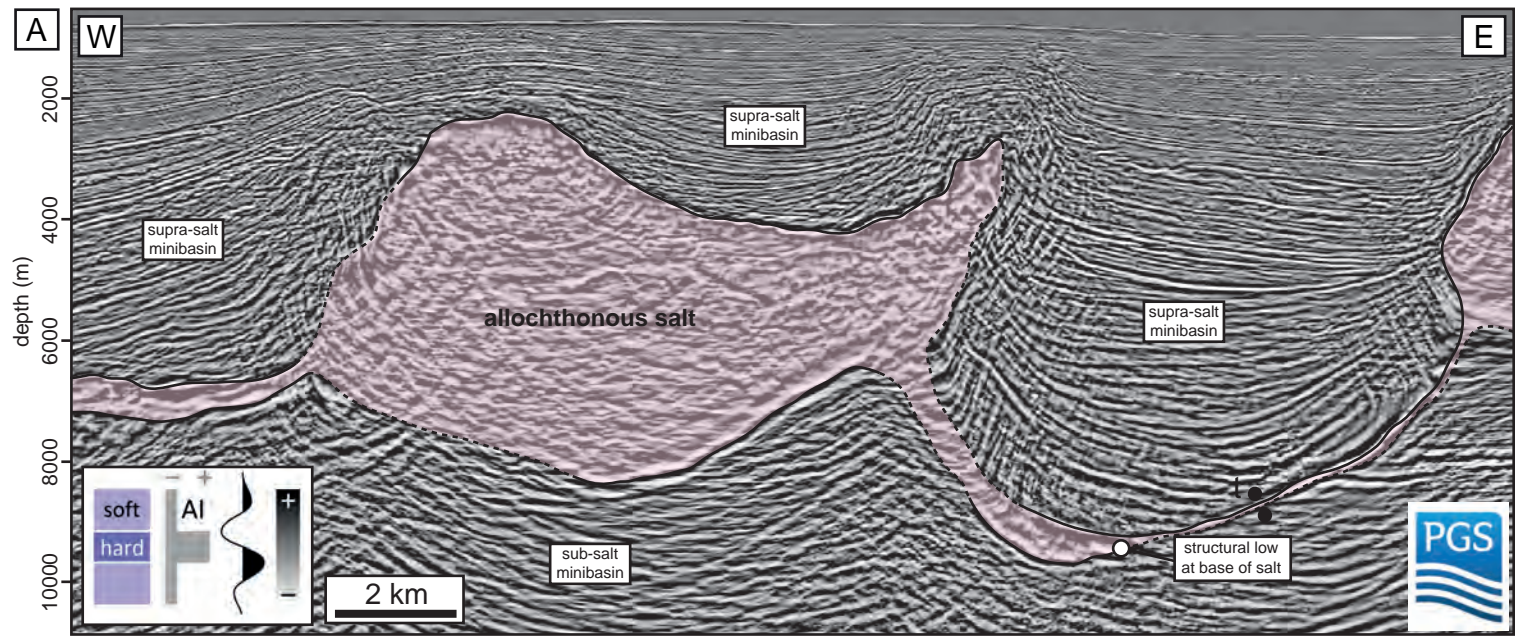


Fig. 4

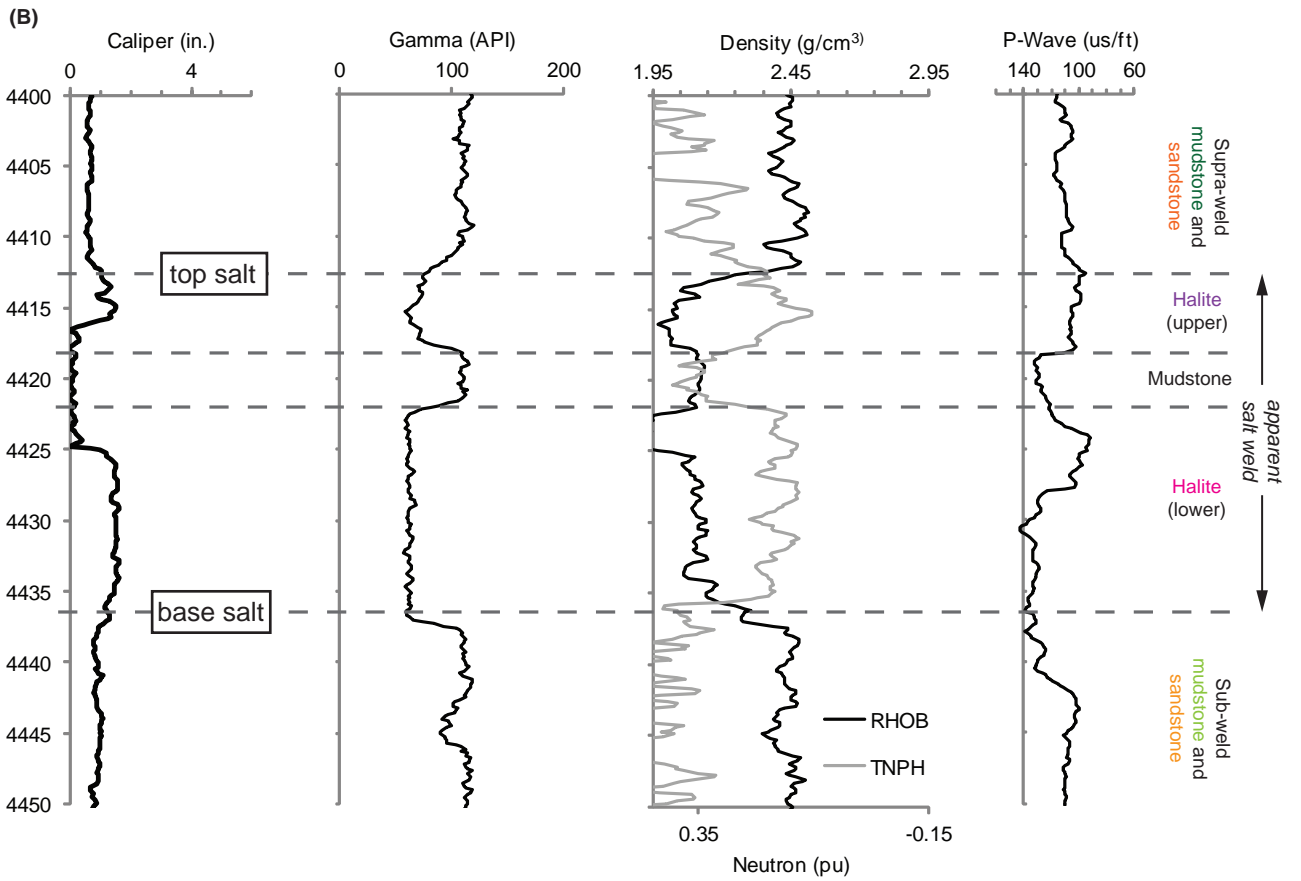
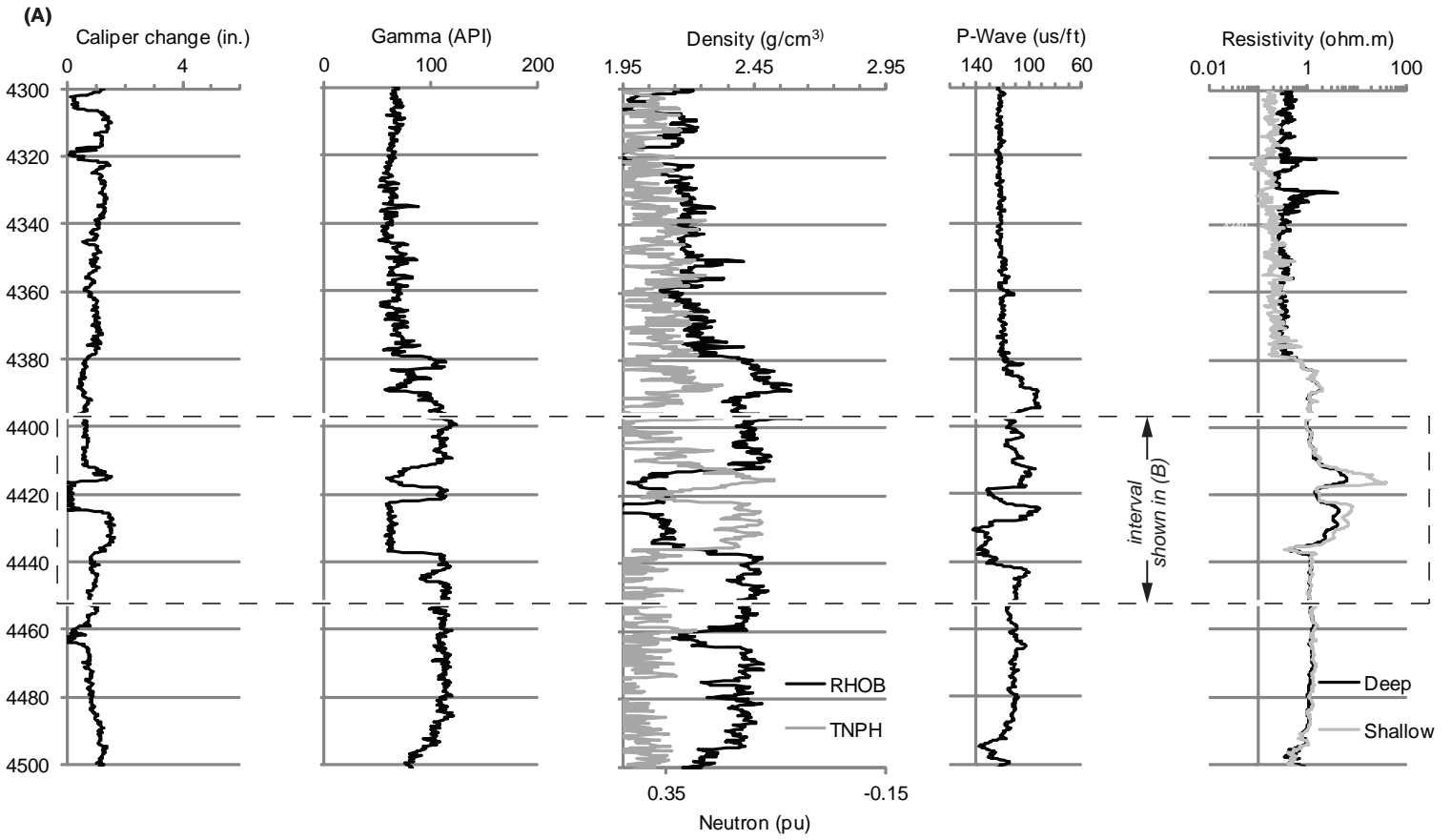


Fig. 5

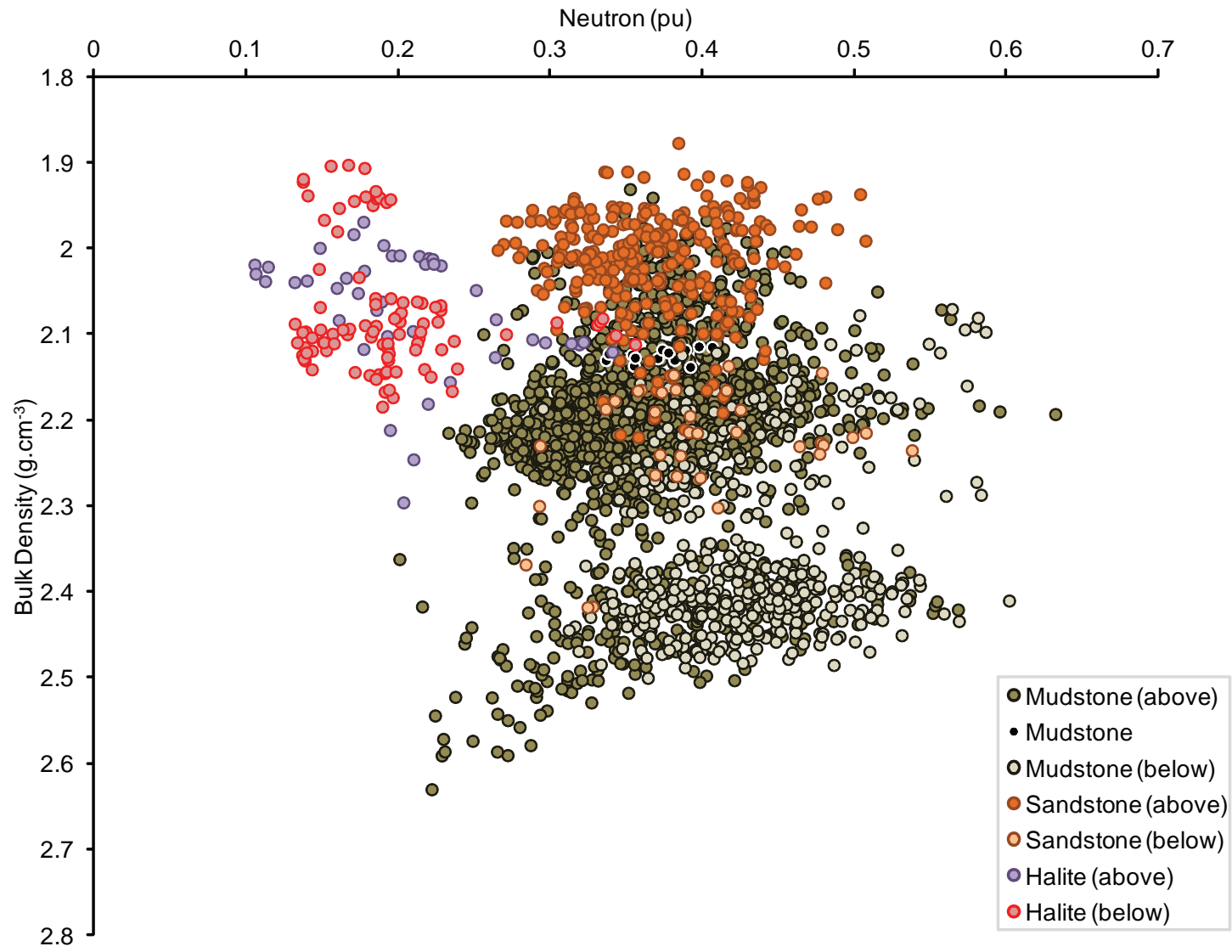


Fig. 6

